SIMULATION AND MODELING OF RESIDUAL STRESSES DUE TO OVERLAY WELDING

Presented
By
Bora Yildirim

A General Examination Report
Presented to the Ph.D. Committee As A Research Proposal

February 1998

Table of Contents Page

Abstract

In this proposal, the importance of the residual stresses in the weld overlay components is expressed. Specifically, some of the aspects on the development of a numerical model to determine the residual stress-strain state due to overlay welding are discussed. Firstly, some background and literature survey is given to address the problem appropriately. This includes numerical models for welding heat sources, simulation of welding using transient thermal and thermo-elasto-plastic formulations, and summary of three papers related to these subjects. In the proposed research, the finite element method will be used to calculate the residual strain and stresses in weld overlay components. The coupling between thermal and mechanical analyses will be neglected. In the thermal analysis, the latent heat effects due to phase changes and solid phase transformations will be considered. In the mechanical model, time-independent thermo-elasto-plastic formulations and transformation plasticity due to phase transformations will be included. Temperature dependent material properties will be used in both analyses. Using these residual stresses, stress intensity factors and strain energy release rates will be calculated for different crack lengths of assumed underclad or other type of cracks. This numerical model might serve for future parametric sensitivity studies of various welding parameters on residual stresses in such overlay welds.

1. Introduction

The stainless-steel piping components of nuclear power plants often suffer intergranular stress-corrosion cracking (IGSCC) in the heat-affected zone of weldment. This is attributed to environmental corrosion, material sensitivity, and applied tensile stress.

According to reports in 1988 by the United States Nuclear Regularity Commission (NRC), a series of methods for elimination or reduction of IGSCC in stainless-steel pipes have been proposed. They include the selection of corrosion-resistant material, the improvement of water quality, and the modification of stress.

For alteration of stress distribution, there are three methods: (1) induction heat stress improvement (IHSI), (2) mechanical stress improvement process (MSIP), and (3) welding overlay repair (WOR). The main purpose of these methods is to introduce compressive residual stress at the inner surface of the piping component. Thus, further intergranular stress corrosion cracking can be prevented in stainless-steel pipes in susceptible corrosion environments.

Among the methods for changing the pipe stress, IHSI and MSIP are commonly used in piping components where crack has not yet occurred or where the crack depth is still shallow in the through-wall direction. When intergranular stress-corrosion cracking is too deep, the crack tip will be situated with in the tensile stresse zone. In this case IHSI or MSIP will greatly enhance the crack growth and therefore would be unsuitable. For piping components with such deeper cracks in the through-wall depth direction, the application of WOR is required.

Black liquor recovery boilers are a critical component in Kraft pulp mills. They provide a means for the mills to recover the chemicals used in the pulping process and to produce process steam which generates a significant portion of the electricity required for mill operation [1,2]. They provide a means for the mills to recover chemicals used in the pulping process and to produce process steam which generates a significant portion of the electricity required for mill operation. Metal tubes are an essential part of a recovery boiler comprising the floor, walls, roof and the superheater. Much of the metal tubing is carbon steel, but because the boiler atmosphere is quite corrosive, composite tubing of stainless steel on carbon steel is used in some areas to provide additional corrosion resistance.

While the use of composite tubes has solved most of the corrosion problems experienced by carbon steel tubes, significant cracking has been reported [2] in the stainless steel layer of composite tubes subjected to service. Metallographic examination indicates that the cracks always initiate at the outer surface and penetrate radially through the stainless steel layer. Nearly always, the cracks stop at or before reaching the interface between the carbon steel and stainless steel layers. However, there are also cases where the cracks propogate along the interface, impeding heat transfer and producing a crevice where corrodents can be trapped. In a few cases, delamination and spalling of chunks of

the stainless steel layer have occurred, resulting in the exposure of the carbon steel core to the boiler atmosphere. The mechanism of cracking is currently the subject of a multi-disciplinary study. Alternate cladding materials, including nickel-based alloys, are being considered. In general industry, especially in the nuclear industry, welding overlay repair is an important repair method mainly used to rebuild piping systems suffering from intergranular stress-corrosion cracking.

Overlay welding is also used to produce a corrosion resistant surface coating on a mild steel shaft substrate. However, when such component is subjected to fluctuating loads in service the fatigue properties, as well as the residual stresses, of the overlay weld are of importance.

Because of the difference in the thermal expansion coefficient of the base metal and deposited metal, and complicated restraint arising from cooling process after welding, significant residual stresses generate in the cladding. The knowledge of the stress profile in the as-welded condition is of prime importance for several reasons. First, fracture mechanics analysis of the vessel should take into account the residual stresses. Second, residual stresses in the stainless steel cladding may increase the tendency for the stress corrosion cracking if their magnitude is sufficient. Finally, the mechanisms of some observed underclad cracking in the heat affected zone could be better understood if the stresses were known in this region during cladding process. During the past ten years, the simulation and numerical modeling of welds and overlay welds have been studied extensively. In the following section a summary of three studies that are related to this phenomenon is given.

2. Literature Review on Simulation and Modeling of residual stresses due to overlay welding

2.1 A New Finite Element Model for Welding Heat Sources

By: John Goldak, Aditya Chakravarti, and Malcolm Bibby

The problems of residual stress and reduced strength of a structure in and around a welded joint or in an overlay weld component are a major concern of welding industry.

These problems result directly from the thermal cycle caused by the localized intense heat input of fusion welding. The high temperatures developed by heat source cause significant metallurgical changes around the weld area of low carbon structural steels. The thermal history, particularly soaking time at high temperatures and cooling time, determines the microstructure and mechanical composition for a given composition. And the cooling time is also a controlling factor in the diffusion of hydrogen and the cold cracking of welds. Accurate predictions of residual stress, distortion, and strength of welded structures require an accurate analysis of the thermal cycle. Therefore a good model for the weld heat source in the analysis of the thermal cycle is an important issue.

John Goldak and his colleagues studied the mathematical models for weld heat sources based on a Gaussian distribution of power density in the space. After examining the performance of several models, they proposed a new heat source model, a double ellipsoidal geometry, that is not only more accurate than those now available but first one capable of handling cases that lack radial symmetry. In addition, the model smoothes the load vector which reduces the error and computing costs of FEM analysis. Also the size and shape of the heat source can easily be changed to simulate both the shallow penetration arc welding processes and the deeper penetration laser and electron beam processes.

The basic theory of heat flow developed by Fourier and applied to moving heat sources by Rosenthal [4] in the late 1930s is still the most popular analytical method for calculating the thermal history of welds. The equation for this model can be written as (see fig.1, equation 1):

$$T - T_0 = \frac{q}{2\pi kg}\sqrt{\frac{\pi k}{vrc_p}}e^{-vc_p(x+r)/2k} \qquad (1)$$

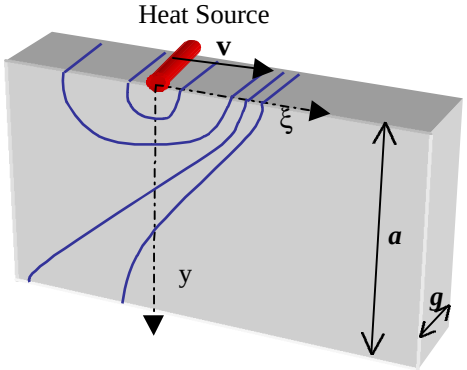

Where k, c_p, v thermal conductiv and specific volume heat content and the rate of fusion respectively and q is the heat input per unit thickness due to welding arc. T_0 is te initial temperature.

Figure 1: Temperature distribution in tin narrow plate due to eat source moving along one of its edges (Rosenthal *et al.*).

But as many researchers have shown, Rosenthal's analysis (which assumes a point, line, or plane source of heat) is subjected to serious error for temperatures in or near the fusion and heat-affected zones. In the regions of the workpiece where the temperature is less than 20% of the melting point, Rosenthal's solution can give quite accurate results. However, the infinite temperature at the heat source assumed in this model and the temperature sensitivity of the thermal properties increases the error as the heat source is approached. Although many of the FEM techniques developed for fracture mechanics (due to similarity of temperature distribution around the heat source to the stress distribution around crack tip) can be adapted to the Rosenthal model, since it would not account for the actual distribution of heat in the arc and would not accurately predict temperatures near the arc, this approach is not commonly used.

Pavelic *et al* [5] suggested another model with a distributed heat source. He proposed a Gaussian distribution of flux (W/m^2) deposited over the surface. The equation for this model can be written as (see figure 2 and equation 2):

$$q(r) = q(0)e^{-Cr^2} \tag{2}$$

Where: $q(r)$ = surface flux at radius r (W/m^2)

$q(0)$ = maximum flux at the center of the heat source (W/m^2)

C= concentration coefficient (m^{-2})

r = radial distance from the center of the heat source.

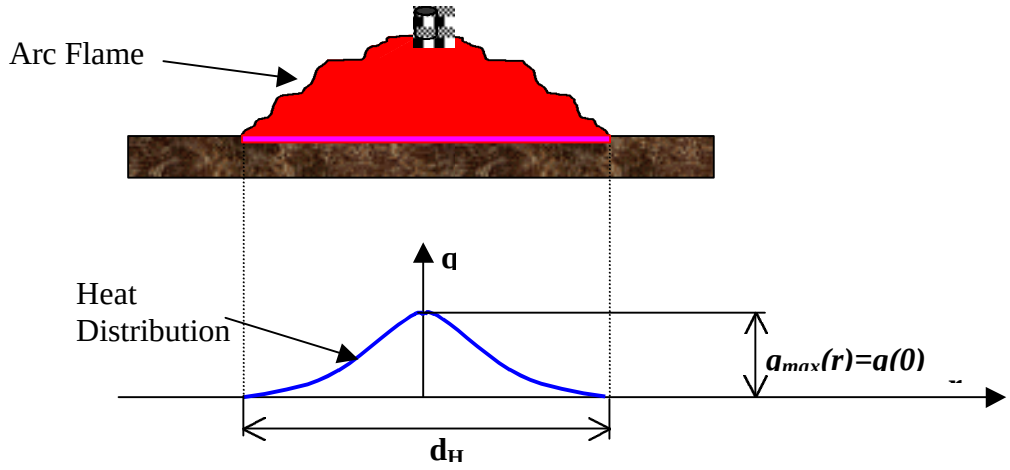

Figure 2: circular disc heat source (Pavelic *et al*.)

Here, C is inversely related to the source width; a more concentrated source would have a smaller width and a larger value of *C*.

An alternative form of Pavelic that is expressed in a coordinate system that moves with the heat source is suggested by Friedmen, Krutz and Segerlind [6] takes the following form (see fig. 2 in [3]):

$$q(r) = \frac{3Q}{\pi c^2} e^{-\frac{3}{c^2}(x^2+\xi^2)} \tag{3}$$

where:Q = energy input rate (W)

c= is the characteristic radius of flux distribution (m) and $\xi = z + v(\tau - t)$

While these models are certainly a significant step forward, it has been suggested that heat should be distributed to the molten zone to reflect more accurately the digging action of arc. These models do not account for the rapid heat transfer of heat throughout the fusion zone. Therefore it has been understood that there is a need for an effective volume source. So for high power density sources such as the laser or electron beam, a hemispherical Gaussian distribution power density (W/m^3) is suggested and it has the following form:

$$q(x,y,\xi) = \frac{6\sqrt{3}Q}{\pi\sqrt{\pi}c^3} e^{-\frac{3}{c^2}(x^2+y^2+\xi^2)} \tag{4}$$

Though this heat source is expected to model an arc weld better than disc source, it has limitations too. Firstly molten pool in many welds is often far from spherical, secondly it is not appropriate for welds that are not spherically symmetric such as deep penetration electron beam, or laser beam welds. To overcome these constraints, an ellipsoidal volume source is proposed and it has the following form (see figure 3 in [3]):

$$q(x,y,\xi) = \frac{6\sqrt{3}Q}{\pi\sqrt{\pi}abc} e^{-3(x^2/a^2+y^2/b^2+\xi^2/c^2)} \tag{5}$$

where *a,b,c* are the semi-axes parallel to coordinate axes *x,y,*ξ . Calculations with this kind of model revealed that temperature gradient in front of the heat source was not as steep as expected and the gentler gradient at the trailer edge of molten pool was steeper

than experimental experience. To overcome this limitation, two ellipsoidal sources are combined as shown fig. 3 in [3]. These combined models have the following form:

$$q_f(x,y,\mathrm{x}) = \frac{f_f\, 6\sqrt{3}Q}{\mathrm{p}\sqrt{\mathrm{p}}abc} e^{-3(x^2/a^2+y^2/b^2+\mathrm{x}^2/{c_1}^2)}, q_r(x,y,\mathrm{x}) = \frac{f_r\, 6\sqrt{3}Q}{\mathrm{p}\sqrt{\mathrm{p}}abc} e^{-3(x^2/a^2+y^2/b^2+\mathrm{x}^2/{c_2}^2)} \quad (6)$$

$$q(x,y,\mathrm{x}) = f_f q_f(x,y,\mathrm{x}) + f_r q_r(x,y,\mathrm{x}), \qquad f_f + f_r = 2 \quad (7)$$

Fractions f_r and f_f of the heat deposited in the front and rear quadrants and four characteristic lengths can be determined if the cross-section of the molten zone is known from experiment. In the absence of better data, a good guess can be made taking the distance in front of the heat source equal to one-half the weld width and the distance behind the heat source equal the twice the width and a estimate of input fractions according to type of welding.

They verified this model considering 2 examples as shown figures 4,5 in [3]. They obtained higher accuracy in the temperature distribution and in the dimensions of FZ and HAZ than the results calculated using previous models (see fig 8 in [3]).

2.2 Numerical Simulation of Welding and Quenching processes using Transient Thermal and Thermo-Eloasto-Plastic Formulations

By: Y. V. L. N. Murthy, G. Venkata and P. Krishna Iyer.

Murthy *at al.* [7] detailed a comphrensive methodology for the analysis of residual stresses due to welding and quenching processes. They have made the following assumptions in their study.

i. Coupling between thermal and mechanical analysis is neglected.

ii. Two-dimensional quasi-steady state models are used instead of three-dimensional models. The accuracy obtained from two-dimensional model is good for high weld speeds, which corresponds to simulating a condition of negligible temperature gradient in the direction of weld.

iii. Trapezoidal type of weld heat input is used to avoid numerical convergence problems due to sudden increase in the temperature.

iv. Temperature field, in the molten weld pool is assumed to be governed by the same equation as that applied to the solid metal region (see eq. 8).

v. Von Mises yield criterion and iso-kinematic hardening model is used to calculate the plastic strain and stresses due to thermal loading.

vi. The effect of creep on the stress relief during the process is assumed to be negligible. It has been shown that the time independent thermo-elasto-plastic modeling together with kinematic hardening would sufficiently estimate the residual stress levels [8].

vii. Overlapping of the weld passes relieves the stresses at temperatures higher than the transformation temperature therefore, an accurate estimation of the location and magnitude of the residual stresses could be obtained analyzing only the last few weld passes.

They have used finite element method in their thermal and mechanical models. With the use of assumption **i**, they first solve the transient thermal problem and find the temperature distribution on the specimen as a function of time. And in a separate model they use these temperatures as the input to calculate the residual stresses.

Their transient analysis can be summarized as follows:

The partial differential equation used for transient heat conduction, with internal heat generation has the following form:

$$\frac{\partial(k(T)\partial T/\partial x)}{\partial x}+\frac{\partial(k(T)\partial T/\partial y)}{\partial y}+\frac{\partial(k(T)\partial T/\partial z)}{\partial z}+\dot{Q}=\rho(T)C(T)\frac{\partial T}{\partial t} \qquad (8)$$

where ρ = density,

C= capacity,

k = thermal conductivity of given material.

All material properties are temperature-dependent, experimentally measured values are used in this analysis. Finite element discretisation of the transient conduction equation can be found in appendix 1a. Heat due to weld torch is applied as uniform distributed surface flux on the weld passes in a trapezoid form as shown figures 5 and 6 in [7].

Surface heat loss due to convection and radiation are combined together as a one-convection boundary condition as shown in equation 2 in [7]. They examined the cross section of the specimen to calculate two-dimensional quasi-steady state temperature, therefore equation 8 takes the form of equation 5 in [7]. A time incremental solution is essential to take care of changes in the temperature with time. Although they used Euler's backward implicit method, a more generic formulation can be found in appendix 1a. They also included latent heat due to phase change and solid phase transformation using heat source method. The details of this method are described in appendix 1b. Flow diagram they followed in their transient thermal analysis can be explained as follows:

(a) Geometry, boundary conditions, material properties and tolerance limit are read from a file into the transient thermal code.

(b) Temperatures are set to the reference values for t=0.

(c) Incremental heat input is done for given t. Since heat source is a function of time this has to be repeated at every time increment.

(d) Effective conductivity and capacity are calculated using the temperature calculated in previous iteration.

(e) Matrices and load vectors are assembled (appendix 1a), temperatures are calculated for given iteration and time $t+\Delta t$.

(f) If the temperature of any node reaches phase change temperature, latent heat is obtained, fictitious heat flow vector and new heat flow vector are calculated, temperatures are reset for given time increment. Residual vector computed and convergence is checked. (i.e. goto (h)).

(g) If the temperature of any node reaches the solid phase transformation:

Firstly, it is checked if this temperature is in the marstensite transformation range? If it is so, using the empirical equation (eq. 9) suggested by Koistinen- Marburger [9], the fraction of martensite is calculated.

$$v_m = 1 - e^{0.11(T - T_m)} \tag{9}$$

where T_m is the martensitic transformation temperature which is around 400 °C. According to this new volume fraction of martensite, fictitious heat flow vector and

new heat flow vector are calculated, temperatures are reset for given time increment. Residual vector computed and convergence is checked. (i.e. goto (h)).

If temperature is not in the martensite transformation range, the volume fractions of bainite, pearlite and ferrite are calculated using Avrami equation, (eq. 10) given in references [9,10].

$$v_k = 1 - e^{(-b_k t^{nk})} \tag{10}$$

Constant b_k 's for each phase can be found in these references. Again, according to this new volume fraction of these phases, fictitious heat flow vector and new heat flow vector are calculated, temperatures are reset for given time increment. Residual vector computed and convergence is checked. (i.e. goto (h)).

(h) Residual vector is calculated and convergence is checked. If the convergence criterion is not satisfied, another iteration needs to be done (i.e. go back to (d)). If the convergence criterion is satisfied continue to (i).

(i) Results are printed out for time $t+\Delta t$, and check is done if steady state or final uniform temperature is reached, if so execution is terminated but if not, execution is continued for the other time increment (i.e. goto (c)).

This completes the thermal analysis and at the end of this analysis the thermal history for each time step is written to a file. In mechanical analysis, they consider the thermal history corresponding to last few welds using assumption vii to calculate residual stresses. They use Von Mises yield criterion in the mechanical analysis, detailed formulation on the constitutive equations used in elastic and plastic ranges can be found in appendix 2. Solid phase transformations from austenite to ferrite, pearlite, bainite and martensite during cooling cause material dilatations locally and contribute to additional strains similar to thermal strains which has the following incremental form:

$$\{d\varepsilon^{ph}\} = 1/3 d\{\Delta V / V^{ph}\}\mathbf{I} \tag{11}$$

where: $\Delta V / V^{ph}$, is the volumetric strain during phase transformation and $\mathbf{I}$ is the identity matrix. A volumetric strain of 0.044 is assumed to have occurred at a region in

the body where 100% austenite is transformed to 100% martensite and a strain of 0.007 if transformed to 100% ferrite/pearlite. Volumetric strains are assumed to be in proportion to the material phases transformed, and with the help of equation 10, these proportions can be calculated.

It has also been observed that during solid phase transformations plastic strains may occur even if the stresses lie well below the elastic limit and are found to be proportional to the rate of transformation and instantaneous deviatoric stress state. This phenomenon, called *transformation plasticity*, is explained to be due to microscopic plasticity created in the weaker phase by volume differences between two phases and is oriented in the direction of applied stress. Two methods are used to introduce transformation in to calculations, which include the use of unusually low yield stress during transformation, or introducing an additional plastic strain term which depends on the volume and rate of the material phases formed and deviatoric stress state. The latter approach is used in this paper. Additional plastic strain, $\{de^{Tp}\}$ due to transformation plasticity is written as:

$$\{de^{Tp}\} = 3K(1-m)dmS_{ij} \tag{12}$$

where: K is the constant defined in [7] pp. 139 for different phases an m is the volume fraction of material phases formed. S_{ij} is the devitoric stress tensor. Since the volumetric strain of ferrite/pearlite is small compared to the volumetric strain of martensite, transformation plasticity contribution from ferrite/pearlite can be neglected. Considering the effect from martensitic transformation only, additional plastic strain, $\{de^{Tp}\}$ due to transformation plasticity can also be written as [12]:

$$\{de^{Tp}\} = \frac{5S_{ij}\Delta V}{4YV}(2-3v_m-\Delta v_m)\Delta v_m \tag{13}$$

where Y is the flow stress in the weaker phase, v_m is the fraction already transformed (see eq. 9) and Δv_m is the amount which transforms during the increment. Finally, total

strain increment can be written as:

$$\{d\varepsilon\} = [M]\{d\varepsilon^{e}\} + [M]\{d\varepsilon^{p}\} + [M]\{d\varepsilon^{Tp}\} + [M]\{d\varepsilon^{ph}\} + [M]\{d\varepsilon^{T}\} \quad (14)$$

Total strain increment

Elastic strain increment

Plastic strain increment

Trans. plasticity strain increment

Volumetric strain increment

Thermal strain increment

Flow diagram they followed in their transient mechanical analysis can be explained as follows:

A. Geometry, boundary conditions, material properties and tolerance limit are read from a file into the transient mechanical code.
B. Temperatures are incremented from the previous equilibrium state, and these are the only external loads input to the body.
C. Iteration starts here.
D. Stiffness matrix and incremental load vector (if it is the first iteration) is calculated as described in appendix 2. If there is a liquid portion at given temperature, zero stiffness is used for that portion.
E. After assembly and solution of equilibrium equation, incremental displacements are obtained. From these displacements, incremental strains are obtained, and if there is a solid phase transformation for the given temperature, transformation plasticity and volumetric incremental strains are calculated according to eq.'s 11-12 for each integration point. The incremental strain calculated from transformation plasticity is added to total plastic strain (since this strain is irreversible) to modify the yield surface later.
F. If there is any plastic strain due to transformation plasticity, the yield surface is modified for given integration point.
G. Incremental stresses and effective stress are calculated. If effective stress is less then the current yield stress, K and the rest of it executed (i.e. no yielding for this integration point at current iteration).
H. If effective stress is greater than current yield stress, incremental plastic strain is calculated and added to the previous plastic strain.
I. Yield stress is calculated from plastic strain.

J. Using a subincrementation scheme excess strain is divided over that corresponding to yielding and modifications are done to incremental stress and strain to reduce the stress points to yield surface.

K. Incremental strains and stresses are added to the total values.

L. Residual load vector is calculated.

M. Convergence is checked. If a convergence criterion is not satisfied, another iteration is needed, incremental loads are replaced with the residual load and C is executed again.

N. If convergence is satisfied, results are printed out and if all load steps are not covered yet, B is executed for another load step. If all load steps are covered, execution is stopped.

They studied two examples; one of them is a single-pass butt welding of a cylindrical pipe made up of carbon-manganese steel with OD 114.3 mm, wall thickness of 8 mm and an overall length of 400 mm. They used isoparametric, 8-noeded elements in their analysis, formulation of these elements can be found in equations 18-19, figure 2 in [7]. The finite element mesh and heat input model used in this study is shown in figure 5 in [7]. Temperatures and stress variations computed are plotted together with the measured values obtained from literature as shown in figures 7-13. They are in a very good agreement with the data obtained from literature.

They also did the analysis of multi-pass welding of two 50-mm thick plates. They used two simplified models in this analysis. Analysis model wit a single layer covering the last six welds passes with the heat input of all the passes applied onto the elements in that layer and analysis of the last weld pass. The finite element meshes and heat input models used in these plate models are shown in figures 14 and 15 in [7]. Some stress distributions are plotted together with the measured values obtained from literature as shown in figures 16-17 and in a very good agreement with the data obtained from literature. The difference can be attributed the type of heat source and arc speed used in this analysis.

2.3 Numerical Analysis of Residual Stress Distribution in Tubes with Spiral Weld Cladding

By: B. Taljat, T. Zacharia, X-L. Wang, J. R. Keiser, R. W. Swindeman, Z. Feng and M. J. Jirinec

Taljat *at al.* [13] studied the residual stresses and strains in a tube with spiral weld cladding. They have used two-dimensional axisymmetric finite elements to determine the residual stresses and strains. Cladding material is Alloy 625 and base metal is SA210 carbon steel tube. The welding process consists of two layers continuously applied in the circumferential direction, resulting in a spiral 360-deg weld cladding (see fig.1 in [13]). The first layer is made with gas metal arc welding process and second layer is made with gas tungsten arc welding process. The purpose of the second layer is to temper the heat-affected zone. Welding parameters used in this analysis are shown in table 1 in [13]. They have also conducted Neutron Diffraction measurements separately in a parallel study. The ND results are compared with FE calculations.

In their finite element analysis they have accounted for convective and conductive heat transfer in the weld pool, weld pool surface and heat conduction into the surrounding material, as well as the conductive and convective heat transfer to the ambient through cooling substances surrounding the tube. Temperature dependent material properties and the effect of latent heat of fusion are also taken into consideration in this study. The assumptions they have made in their analysis can be summarized as follows:

i). An axisymmetric model is considered because of the circumferental welding direction. This assumption considerably simplifies the modeling effort and reduces the computational time.

ii). Thermal and mechanical analyses are assumed to be uncoupled and performed in two separate runs.

iii). To account for heat transfer effects due to fluid flow in the weld pool, an increase in the thermal conductivity above the melting temperature is assumed.

iv). The overall heat flux is calculated as $Q = \eta VI$ where, η represents the efficiency factor, V is voltage and I is electric current.

v). The heat flux distribution is assumed to be single ellipsoidal power density distribution and has the following form in cylindrical coordinates :

$$q(r,\phi_r,z) = \frac{6\sqrt{3}Q}{\pi\sqrt{\pi}abc} e^{-3(r^2/a^2+\phi_r^2/b^2+z^2/c^2)} \tag{15}$$

where r,ϕ_r,z are the radial, tangential and axial coordinates respectively. Constants *a, b, c* represent the characteristic dimensions of arc as described in section 2.1. Because the axisymmetric model is assumed, tangential coordinate can be fixed using the following relation:

$$\left(\frac{\phi_r}{b}\right)^2 = \left(\frac{v}{b}\right)\left(t - \frac{t_t}{2}\right)^2 \tag{16}$$

vi). Radiant heat transfer is assumed at the outside tube surface and the value of 0.2 is used for emissivity coefficient.

vii). Because of the axisymmetric model assumption, the heat is simultaneously applied and the material is simultaneously applied and the material is simultaneously melted and deposited around the circumference.

viii). Transformation plasticity and phase change effects due to rapid cooling are not included in the mechanical analysis.

Material properties used in this analysis are shown as a function of temperature in figures 3-5 in [13]. Finite element mesh and geometry used in this study are shown in figure 2 in [13]. Six welding passes are simulated to obtain a weld of sufficient length and to get a uniform region of residual stresses that are unaffected by ten beginning and end of the welding process. In the thermal analysis, after the first layer is finished, tube is cooled to room temperature, and then the second weld layer started. In the second layer, computational steps contain only heating and cooling because no filler material is to be added. After the last (sixth) pass of the second layer, the tube is again cooled to room temperature. All of the temperature history is kept in a file to use in mechanical analysis. In the mechanical analysis, an elasto-plastic constitutive law is used. The same mesh is used for both analysis and thermal data obtained from the transient thermal is the only external load input to the mechanical analysis. Figure 6 in [13] shows comparison of strains measured and calculated for the cross sections shown in figure 2 in [13]. Figure 7 in [13] shows the radial stress are compressive and their magnitude is not significant.

Axial residual stress in the weld cladding are tensile and lower than the yield stress, compressive at approximately one third of the tube thickness as shown in figure 8 in [13]. Figure 9 in [13] shows that the calculated tangential residual stress distribution is similar. Finite element results show that the whole tube is plastically deformed during the welding process and effective plastic strain as a function of radial position is shown in figure 10 in [13]. Authors also conclude that annealing relieves the residual stresses to almost zero.

3. Proposed Research

Overlay welding is often used to produce a corrosion resistant surface coating on nuclear reactor vessels, light water reactor pressure vessels, stainless-steel piping components, and mild steel shafts, and metal tubes of recovery boilers. While overlay welding has solved most of the corrosion problems, significant cracking has been reported in and under the clads. Indeed the failure of an overlay-welded shaft by the propagation of a crack from the overlay weld is sometimes observed. Metallographic examination indicates that the crack always initiate at the outer surface and penetrate radially through weld overlay layer. Nearly always, the cracks stop at or before reaching the interface between substrate and layer. However, there are also cases where the cracks propagate along the interface, impending heat transfer and producing a crevice where corrodents can be trapped. In a few cases, delimination and spalling of chunks of the overlay layer on metal tubes of recovery boilers have occurred, resulting in the exposure of the carbon steel core to the boiler atmosphere. To be able to analyze these cracks, residual stresses in the weld and substrate must be predicted accurately. Up to now, numerical models developed for this calculations have not included all the details of a welding processes (advanced heat source, phase transformation, transformation plasticity) as described in section 2.2. Although P. Dupas *at al.* [11] and B. Taljat *at al.* [13] (as described in section 2.3) conducted an analysis to determine the cladding residual stresses, they did not take the micro structural changes and transformation plasticity into consideration in their study. As discussed in [12] by Goldak *at al*. Phase changes and transformation plasticity have a significant effect on the residual stresses generated by welding and should be included in the analysis.

There are also some studies on crack propagation in overlay welds [16], but again they used simple theoretically derived residual stresses and considered edge cracks only in the weld. Different crack configurations and interface cracks should be considered together with an accurate stress analysis.

The proposed research can be summarized as follows:

- Finite element method and a self-developed code will be used to simulate transient thermal behavior of the overlay welding will be done for various geometries. As the heat source gas metal arc welding and laser welding will be simulated. Temperature dependent material properties, latent heat change due to phase change and solid phase transformation will be taken in to account in the analysis (as described in appendix a and appendix b).
- Transient temperature distribution, depth of the fusion zones (FZ) and heat-affected zones (HAZ) (see figure 3) will be calculated for given material couple and will be compared to data available in the literature. There is not much data available on overlay welds in literature.

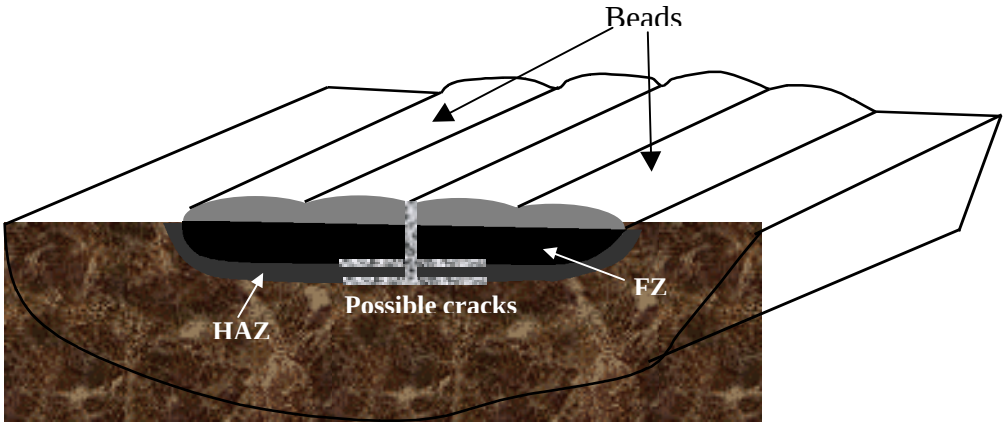

Figure 3: A schematic representation of overlay weld and possible crack locations.

- Assuming that coupling between thermal and mechanical analysis, therm-elasto-plastic analysis of overlay weld will be done, using the transient temperature data

obtained from the thermal simulation as input. In this analysis, solid phase transformations, transformation plasticity, volumetric strains will also be taken into consideration using the empirical formulas available in the literature. Von Mises criterion together with iso-kinematic (see appendix 2) hardening rule in the plasticity analysis.

- Residual stresses will be calculated and stored in a file to be used in fracture analysis.
- As metallographic examination indicates that the crack always initiate at the outer surface and penetrate radially through weld overlay layer, therefore using the same geometry and the residual stress calculated in thermo-elasto-plastic analysis, firstly edge cracks will be analyzed. Linear elastic fracture mechanics (LEFM) assumption will be used. Stress intensity factors and strain energy release rates will be calculated for various crack lengths *a* (see fig. 4), using enriched finite elements [17].
- Metallographic examination also shows that these cracks may turn into T-shaped cracks at Substrate/HAZ or HAZ/FZ interfaces. Therefore these cases will also be considered and stress intensity factors and strain energy release rates will be calculated for various crack lengths *b* (see fig. 4) using enriched finite elements [17].
- These calculations will be repeated for various material couples and geometries.

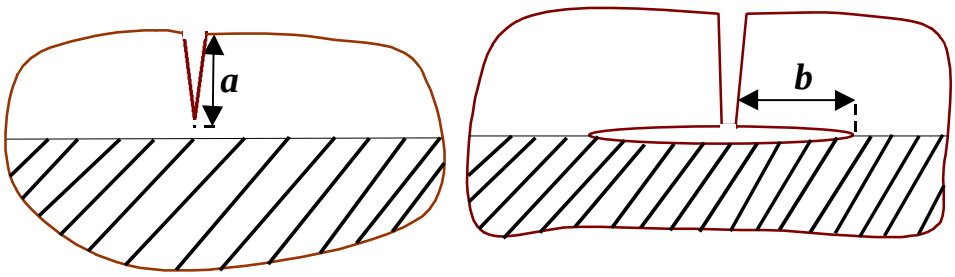

Figure 4: A schematic representation of edge and T-shaped cracks.

4. References

[1] J.R. Keiser, B. Taljat, X.-L. Wang, P.J. Masiasz, C.R. Hubbard, R.W. Swindeman, D.L. Singbeil, R. Prescott, in: Proceedings of 1996 TAPPI Eng. Conf., TAPPI pres, Atlanta, GA,1996, pp. 693-704.

[2] D.L. Singbeil, R. Prescott, J. R. Keiser, R.W. Swindeman, "Composite Tube Cracking in Kraft Recovery Boilers," A state-of-art Review, Technical Report, Pulp and Paper Research Institute of Canada, August 1996.

[3] John Goldak, Aditya Chakravarti, Malcolm Bibby, " A New Finite Element Model for Welding Heat Sources," Metallurgical Transactions B, Volu. 15B, June 1984, pp. 299-305.

[4] D. Rosenthal: *Trans. ASME,* 1946, vol. 68, pp. 849-65.

[5] V. Pavelic, R. Tanbakuchi, O.A. Uyehara, and P.S. Myers: *Welding Journal Research Supplement,* 1969, vol. 48, pp.295-305.

[6] G. W. Krutz and L.J. Segerlind: *Welding Journal Research Supplement,* 1978, vol 57, pp. 211-216.

[7] Y. V. L.N. Murthy, G. Venkata Rao and P. Krishna Iyer,"Numerical simulation of welding and quenching processes using transient thermal and thermo-elasto-plastic formulations," *Computers & Structures ,* Vol. 60 No. 1. Pp. 131-154, 1996.

[8] F.G. Rammerstorfer, D. F. Fischer, W. Mitter, K.J. Bathe and M. D. Snyder, "On thermo-elastic-plastic analysis of heat treatment process including creep and phase changes," *Computers & Structures* Vol. 60 No. 1. Pp. 131-154, 1996.

[9] D. P. Koistinen and R. E. Marburger, "A general equatuion prescribing extent of austenite-martensite transformation in pure iron-carbon alloys and carbon steels," *Acta Metall.* 7,59 (1959).

[10] M. Avrami, "Kinetics of phase changes II," *J. Cem. Phys.* 8,212 (1940).

[11] P. Dupas, D. Moinereau, "Evaluation of Cladding Residual Stresses in Clad Blocks by Measurements and Numerical Simulations," Jornal De Physique IV, vol. 6, jan. 1996 pp 187-196.

[12] A.S. Oddy, J.A. Goldak and J. M. J. McDill," Transformation plasticity and residual stresses in single pass repair welds," Weld Residual Stresses and Plastic Deformation, ASME vol. 173 pp 13-18 (1989).

[13] B. Taljat, T. Zacharia, X-L. Wang, J. R. Keiser, R. W. Swindeman, Z. Feng and M. J. Jirinec, "Numerical Analysis of Residual Stress Distribution in Tubes with Spiral Weld Cladding,", Research and Development, August 1998, pp 328-335.

[14] T.J.R. Hughes, " Analysis of transient algorithms with particular reference to stability behaviour," *Computational methods for transient analysis*, Elsevier Science Publishers,1983, pp 145.

[15] Mendelson, *Plasticity: Theory and Application*, Macmillan, New York (1968).

[16] K. Kalligerakis, B. G. Mellor, " Fatigue Crack Propagation Studies in Stainless Steel Overlay Welds," Int. J. for the Joining of Materials 9 (1) 1997 pp 10-14.

[17] A.C. Kaya and H.F. Nied, "Interface Fracture Analysis of Bonded Ceramic Layers using enriched finite elements", The American Society of Mechanical engineers, Book No. H00853-1993 p. 47-66.

Proposal Budget

	Year 1	Year 2	Year 3	Total
Principal Investigator, 1.O S.	$5,555	$5,777	$6,008	$17,340
Graduate Research Asst. Stipend	12,600	13,104	13,628	39,332
Graduate Research Asst. Tuition	8,300	8,632	8,977	25,909
Employee Benefits	2,284	2,375	2,470	7,129
Total Salaries and Wages	28,739	29,888	31,083	89,710
Research Equipment	8,000	0	0	8,000
Travel	1,500	1,500	1,500	4,500
Materials and Supplies	500	500	500	1,500
Publications	1,000	1,000	1,000	3,000
Communications	500	500	500	1,500
Total Direct Costs	40,239	33,388	34,583	108,210
Indirect Costs (53.5%)	12,927	13,244	13,699	39,870
TOTAL PROPOSED COSTS	$53,166	$46,632	$48,282	$148,080

Budget Notes

1. The tuition rate for academic year 99/00 has been set at $830 per credit. The tuition budgeted is for 10 credits per semester per graduate research assistant. Lehigh University will provide a partial tuition scholarship as part of its commitment to this project.

2. Employee benefits are direct-charged as a percentage of salaries and wages at rates set by HHS Audit Office Negotiation Agreement. The negotiated rate for full-time staff is 37% for FY 98/99 and 36% for FY 99/00. The rate for part-time employee is 9% for both years. The 9% rate is also applied to graduate research assistant's stipend during the three summer months.

3. Travel funds are requested for the principal investigators and the students to attend and present papers at professional society meetings.

4. As the research equipment, a workstation will be purchased for the finite element analysis.

5. Indirect costs are charged as a percentage of modified total direct costs (MTDC) at a rate of 53.5% for FY 98/99 set by HHS Audit Office Negotiation Agreement. This rate is used for future years. Indirect costs are not charged on equipment, tuition and subcontract charges over $25,000.

Appendix 1a

Finite Element Analysis of Transient Heat Transfer Problems

The governing differential equation can be written as follows:

$$\frac{\partial(k(T)\partial T/\partial x)}{\partial x}+\frac{\partial(k(T)\partial T/\partial y)}{\partial y}+\dot{Q}+\dot{Q}_{Lat}=\rho(T)C(T)\frac{\partial T}{\partial t} \tag{1.1}$$

In each element, the approximate solution assumes the form of a linear combination of prescribed shape functions, thus

$$\overline{T}=\sum_{i=1}^{10,12}N_i T_i \tag{1.2}$$

where N_i is the shape functions (appendix 3) and T_i is the nodal temperature values. Using Galerkin method and equation 1.2, equation 1.1 can be rewritten as:

Terms coming from heat flux or convection boundary conditions

$$\int_{\Omega_e}\rho cN_iN_j\,dxdy\left\{\frac{\partial T}{\partial t}\right\}_j+\int_{\Omega_e}\left[\frac{\partial N_i}{\partial x}k_x\frac{\partial N_j}{\partial x}+\frac{\partial N_i}{\partial y}k_y\frac{\partial N_j}{\partial y}\right]dxdy\,\{T\}_j=\int_{\Omega_e}N_i(\dot{Q}+\dot{Q}_{Lat})dxdy+\int_{\Gamma}N_i\bar{q}\,d\Gamma \tag{1.3}$$

Equation 1.3 can be written as:

$$C\dot{T}+KT=F \tag{1.4}$$

Considering temperature and time dependent properties, equation 1.4 can be written as:

$$C(T,t)\dot{T}+K(T,t)T=F \tag{1.5}$$

And with the use of generalized mid-point family methods [14], equation 1.5 can be written as:

$$C(T_{n+\alpha},t_{n+\alpha})\dot{T}_{n+\alpha}+K(T_{n+\alpha},t_{n+\alpha})T_{n+\alpha}=F_{n+\alpha} \tag{1.6}$$

where n represents the nth timestep,

$$\begin{aligned}T_{n+\alpha}&=(1-\alpha)T_n+\alpha T_{n+1}\\ \dot{T}_{n+\alpha}&=\frac{T_{n+1}-T_n}{\Delta t}\\ t_{n+\alpha}&=t_n+\alpha\Delta t\end{aligned} \tag{1.7}$$

Substituting equation 1.7 into equation 1.6, we obtain,

$$\left[\frac{C_{n+\alpha}}{\Delta t}+\alpha K_{n+\alpha}\right](T_{n+1})=\left[\frac{C_{n+\alpha}}{\Delta t}-(1-\alpha)K_{n+\alpha}\right](T_n)+(F_{n+\alpha}) \tag{1.8}$$

No calculation of derivatives is necessary for this method. By changing the values of α from 0 to 1, different members of this family of methods are identified, i.e.,

$\alpha = 0$ -Forward Difference or Forward Euler.

$\alpha = \frac{1}{2}$ -Midpoint rule or Crank Nicolson.

$\alpha = \frac{2}{3}$ -Galerkin.

$\alpha = 1$ -Backward Difference or Backward Euler.

All, except the first (forward Euler), of the above schemes are implicit, i.e., they require matrix inversion for the solution.

In nonlinear problems, convergence criterion can be set as:

$$\sqrt{\frac{\left[\sum_{k=1}^{N}\left\|T_k^i\right\|^2-\left\|T_k^{i-1}\right\|^2\right]}{\sum_{k=1}^{N}\left\|T_k^1\right\|^2}} \le Tolerance \tag{1.9}$$

Appendix 1b

Heat Source Method for Modeling Phase Transformation

A fixed mesh method, which is gaining favor, is the *Fictitious Heat-Flow Method*. This is also referred to as the *heat source* method, as will be done here. We can write heat source or sink term $\dot{Q}_L$ in the equation 1.1 can be written as:

$$\dot{Q}_L = \rho \frac{d\left[\int_\Omega L d\Omega\right]}{dt} \tag{1.10}$$

where ρ is the density and L is the latent heat. We can write equation 1.10 in discritaized form as follows:

$$\dot{Q}_{l,total,k} = \frac{m_k L}{\Delta t} \tag{1.11}$$

where m_k is mass associated with node k obtained from element mass using weighing coefficients. Considering a node k if the temperatures ${}^{t}T_k$ and ${}^{t+\Delta t}T_k^i$ (at the end of iteration i) correspond to the phase change interval, then the latent heat produced at node k due to phase change is given by

$$\Delta \dot{Q}_{l,k}^{i} = \frac{\left[T_{Phase2} - {}^{t+\Delta t}T_k^i\right]}{\Delta t} C^* m_k \tag{1.12}$$

where

$$C^* = \frac{1}{\left[\frac{T_{phase2} - T_{phase1}}{L} + \frac{1}{C}\right]} \tag{1.13}$$

Fictitious heat flow at node k added to net flow vector on the right-hand-side of the equilibrium for successive iterations is obtained by

$$\dot{Q}_{lat,k}^{i} = {}^{t+\Delta t}\dot{Q}_{lat,k}^{i-1} + \Delta \dot{Q}_{l,k}^{i} \tag{1.14}$$

To accelerate the convergence, temperature ${}^{t+\Delta t}T_k^i$ can be reset as:

$${}^{t+\Delta t}T_k^i = T_{Phase1} + \frac{\Delta Q_{l,k}^{i}}{Q_{l,total,k}} (T_{Phase2} - T_{Phase1}) \tag{1.15}$$

Accumulated latent heat at the node is calculated as:

$$\dot{Q}_{acc,k} = \sum \Delta \dot{Q}_{l,k}^{i} \tag{1.16}$$

The heat sink/source vector in equation 1.3 is updated and a solution is found imposing temperatures, as obtained by equation 1.15, at nodes where phase change occurred. The procedure of including a fictitious heat flow vector in the equilibrium equation ceases once the accumulated latent heat over all iterations exceeds the total latent heat available.

Appendix 2

Finite Element Formulation Thermo-Elasto-Plastic Problems

The stress-strain relation for thermo-elasto-plastic analysis is given by

$$\{\sigma\} = [D]\{\varepsilon_e\} = [D]\{\{\varepsilon\} - \alpha(T - T_0) - \varepsilon_p\} \tag{2.1}$$

where $[D]$ is the material matrix, ε_p is the plastic strain. The incremental form can be written as:

$$\{d\sigma\} = [D]\{\{d\varepsilon\} - \alpha dT - \{T - T_0\}d\alpha - d\varepsilon_p\} + [dD]\{\varepsilon_e\} \tag{2.2}$$

Incremental plastic strain is derived as follows:

$$F(\sigma, q, \sigma_0) = 0 \tag{2.3}$$

where F is the yield function and σ_0 is a measure of the size of the yield surface. The size of the yield surface can be treated as a function of accumulated magnitudes of plastic strain E_p and temperature T. i.e.

$$\sigma_0 = \sigma_0(E_p, T) \tag{2.4}$$

Generally the shape, size and position of the yield surface, changes with progress of plastic deformation of the material, indicating strain hardening. In the case of isotropic hardening the assumption is that only the size of the yield surface increases without any change in its position on subsequent flow (see Figure 2.1).

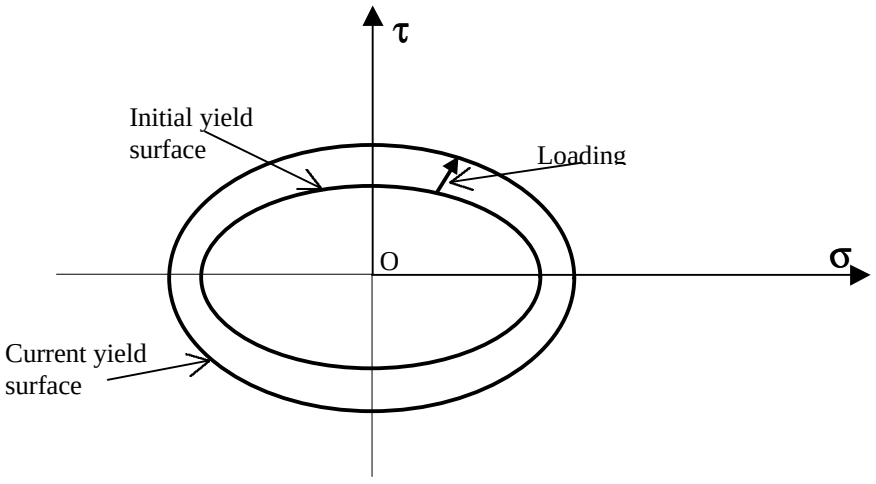

Figure 2.1: Isotropic strainhardening.

In the case of kinematic hardening, the position of the yield surface changes with the yield surface changes with plastic deformation, while the size remains unaltered (see Figure 2.2).

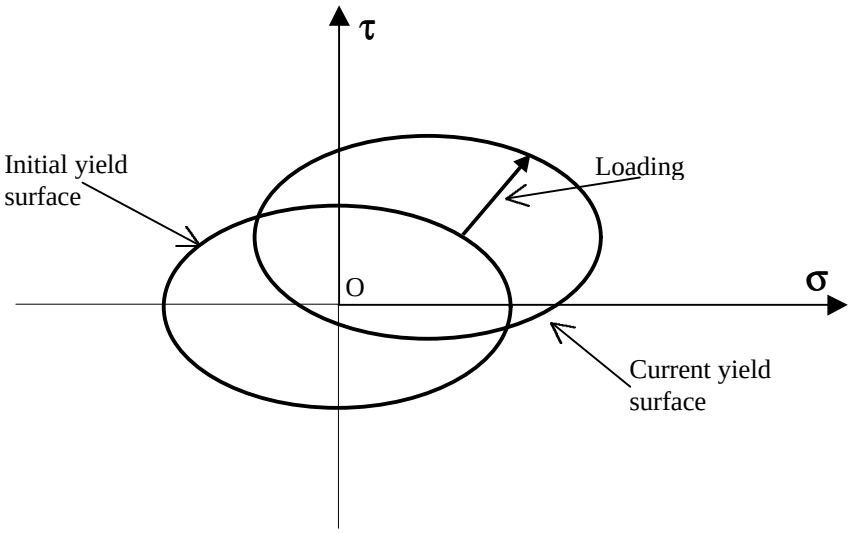

Figure 2.2: Kinematic strain hardening.

It is noticed that [15] cycling loading of the material during load variations is actually represented by a combination of these two types of hardening theories due to Bauschinger effect. For a combined hardening case the yield surface is given by

$$F(\sigma, q, \sigma_0) = f(\sigma - q) - \sigma_0(E_p, T) = 0 \tag{2.5}$$

Subsequent to a load increment, $dF > 0$ represents yielding and $dF < 0$ represents elastic unloading, while $dF = 0$ corresponds to neutral loading. Hence onset of yielding $F = 0$ and $dF = 0$ i.e.

$$dF = \left(\partial f / \partial \sigma^*\right)^T d(\sigma - q) - \left(\partial \sigma_0 / \partial E_p\right) dE_p - \left(\partial \sigma_0 / \partial T\right) dT = 0 \tag{2.6}$$

where $\sigma^* = (\sigma - q)$ and translation of the yield surface is in the direction of plastic strain increment can be written as:

$$dq = \frac{2H}{3} d\varepsilon_p \left(1 - \chi\right) = \frac{2H}{3} dE_p \, n \left(1 - \chi\right) \tag{2.7}$$

where x *is* a fraction indicating the extent of isotropic hardening. x=1 for isotropic hardening and x=0 for kinematic hardening. And *H* is defined as $H = \frac{d\bar{\sigma}}{d\bar{E}_p}$ and $^{-}$ is the

$$dF = \left(\partial f / \partial \sigma^*\right)^T \left(d\sigma - \frac{2H}{3} dE_p n\left(1 - \chi\right)\right) - \left(\partial \sigma_0 / \partial E_p\right) dE_p - \left(\partial \sigma_0 / \partial T\right) dT = 0 \quad (2.8)$$

Considering von Mises yield criterion

$$f = J_2' = \frac{1}{2} \sigma'_{ij} \sigma'_{ij} \quad (2.9)$$

And the current yield stress is defined as follows:

$$Y = Y_0 + \chi H E_p^e \quad (2.10)$$

$$\sigma_0 = Y^2 / 3 \quad (2.11)$$

The unit vector is defined as:

$$n = \frac{\left(\partial f / \partial \sigma^*\right)}{f_m}$$
$$f_m = \sqrt{\left(\partial f / \partial \sigma^*\right)^T \left(\partial f / \partial \sigma^*\right)} \quad (2.12)$$

$$\left(\partial f / \partial \sigma^*\right)^T = \left(\partial J_2' / \partial \sigma^*\right) = \left[\sigma'^*_{11}, \sigma'^*_{22}, \sigma'^*_{33}, \sigma'^*_{12}, \sigma'^*_{23}, \sigma'^*_{31}\right] \quad (2.13)$$

and σ'^*_{mn} can be written as

$$\sigma'^*_{mn} = \left(\sigma'_{mn} - \alpha_{mn}\right) \quad (2.14)$$

The effective plastic strain increment can be written as

$$d\bar{E}_p = \sqrt{2/3}\, dE_p \quad (2.15)$$

From equations 2.10 and 2.11 we can write

$$\frac{\partial \sigma_0}{\partial E_p} = \left[\frac{2}{3}\right]^{\frac{3}{2}} Y H \chi \quad (2.16)$$

$$\frac{\partial \sigma_0}{\partial T} = \left[\frac{2Y}{3}\right] \frac{\partial Y}{\partial T} \quad (2.17)$$

Thus equation 2.8 can be written as

$$\{n\}^T f_m(\{d\sigma\} - \frac{2H}{3} dE_p \{n\}(1-\chi)) = \frac{2Y}{3}\left(\frac{\partial Y}{\partial T}\right)dT + \sqrt{\frac{2}{3}} H\chi dE_p \tag{2.18}$$

Eliminating $\{d\sigma\}$ from equations 2.18 and 2.2, we can obtain:

$$dE_p = \frac{\{n\}^T[D]\{d\varepsilon\} - \{\alpha\}dT - (T-T_0)\{d\alpha\} + \{n\}^T[dD]\{\varepsilon_e\} - 2/3Yf_m^{-1}(\partial Y/\partial T)dT}{S} \tag{2.19}$$

where

$$S = \{n\}^T[D]\{n\} + 2/3(1-\chi) + 2Y/3 f_m^{-1}\chi H\sqrt{2/3} \tag{2.20}$$

and incremental stress can be written as:

$$\{d\sigma\} = [D]\{d\varepsilon\} - \alpha dT - \{T-T_0\}d\alpha + [dD]\{\varepsilon_e\} - \left(\frac{\{n\}^T[D]\{d\varepsilon\} - \{\alpha\}dT - (T-T_0)\{d\alpha\} + \{n\}^T[dD]\{\varepsilon_e\} - 2/3Yf_m^{-1}(\partial Y/\partial T)dT}{S}\right) \tag{2.21}$$

or rearranging it

$$\{d\sigma\} = [D_p]\{d\varepsilon\} - \alpha dT - \{T-T_0\}d\alpha + \left(dD - \frac{[D]\{n\}^T[dD]}{S}\right)\varepsilon_e + \left(\frac{[D]\{n\}2/3Yf_m^{-1}(\partial Y/\partial T)dT}{S}\right) \tag{2.22}$$

where

$$D_p = [D] - \frac{[D]\{n\}\{n\}^T[D]}{S} \tag{2.23}$$

Variation of Y with respect to temperature T can be written as:

$$\left(\frac{\partial Y}{\partial T}\right)dT = \left(\frac{\partial Y_0}{\partial T}\right)dT + \chi\left(\frac{\partial(H\bar{E}_p)}{\partial T}\right)dT \tag{2.24}$$

Using principle of virtual work finite element formulation can be derived as follows:

$$\int_{vol} B^T\{d\sigma\}dvol = dR \tag{2.25}$$

$$\int_{vol} B^T [D_p] B \, dvol = dR + \int_{vol} B^T \left([D_p] \left(d\varepsilon - \alpha dT - (T - T_0) d\alpha \right) - \sigma dD - \frac{[D] \ln(\varepsilon_e^T [dD])}{S} \varepsilon_e - \frac{[D] \ln(2/3 Y f_m^{-1} (\partial Y / \partial T) dT)}{S} \sigma \right) dvol \quad (2.26)$$

Convergence criterion can be written as follows:

$$\sqrt{\frac{\sum_{r=1}^{N} \left(F_{applied}^{i} - F_{calculated}^{i} \right)_r^2}{\sum_{r=1}^{N} \left(F_{applied}^{1} - F_{calculated}^{1} \right)_r^2}} \leq Tolerance, \text{ or } \sqrt{\frac{\sum_{r=1}^{N} \left(\Delta F^i \Delta u^i \right)_r}{\sum_{r=1}^{N} \left(\Delta F^1 \Delta u^1 \right)_r}} \leq Tolerance \quad (2.27)$$

where N is the total node number, i is the iteration number, ΔF and Δu are the incremental forces and displacements respectively.